1-1-2011

One-dimensional multiferroic bismuth ferrite fibers obtained by electrospinning techniques

Avinash Baji
(CAMT)The University of Sydney, Sydney, NSW

Yiu-Wing Mai

Qian Li
Australian National University, Canberra

Shing-Chung Wong
The University of Akron, Akron

Yun Liu
The Australian National University

See next page for additional authors

One-dimensional multiferroic bismuth ferrite fibers obtained by electrospinning techniques

2011 Nanotechnology 22 235702

(http://iopscience.iop.org/0957-4484/22/23/235702)

Nanotechnology **22** (2011) 235702 (6pp) doi:10.1088/0957-4484/22/23/235702

One-dimensional multiferroic bismuth ferrite fibers obtained by electrospinning techniques

Avinash Baji[1,5], Yiu-Wing Mai[1], Qian Li[2], Shing-Chung Wong[3], Yun Liu[2] and Q W Yao[4]

[1] Centre for Advanced Materials Technology (CAMT), School of Aerospace, Mechanical and Mechatronic Engineering, The University of Sydney, Sydney, NSW 2006, Australia
[2] Research School of Chemistry, Australian National University, Canberra, ACT 0200, Australia
[3] Department of Mechanical Engineering, The University of Akron, Akron, OH 44325-3903, USA
[4] Institute for Superconducting and Electronic Materials, University of Wollongong, Northfields Avenue, NSW 2522, Australia

E-mail: avinash.baji@sydney.edu.au

Received 14 February 2011, in final form 14 March 2011
Published 11 April 2011
Online at stacks.iop.org/Nano/22/235702

Abstract

We report the fabrication of novel multiferroic nanostructured bismuth ferrite ($BiFeO_3$) fibers using the sol–gel based electrospinning technique. Phase pure $BiFeO_3$ fibers were prepared by thermally annealing the electrospun $BiFeO_3$/polyvinylpyrrolidone composite fibers in air for 1 h at 600 °C. The x-ray diffraction pattern of the fibers ($BiFeO_3$) obtained showed that their crystalline structures were rhombohedral perovskite structures. Both scanning electron microscopy (SEM) and transmission electron microscopy (TEM) images revealed that the $BiFeO_3$ fibers were composed of fine grained microstructures. The grains were self-assembled and self-organized to yield dense and continuous fibrous structures. The magnetic hysteresis loops of these nanostructured fibers displayed the expected ferromagnetic behavior, whereby a coercivity of ∼250 Oe and a saturation magnetization of ∼1.34 emu g^{-1} were obtained. The ferroelectricity and ferroelectric domain structures of the fibers were confirmed using piezoresponse force microscopy (PFM). The piezoelectric hysteresis loops and polar domain switching behavior of the fibers were examined. Such multiferroic fibers are significant for electroactive applications and nano-scale devices.

1. Introduction

One-dimensional nanostructures have received considerable attention due to their tunable physical and electroactive properties, such as mechanical strength, stiffness, ferromagnetism, ferroelectricity, etc [1–9]. In particular, nanostructured magneto-electric (ME) multiferroic materials with the coexistence of electric and magnetic order parameters are of great scientific and technological interest [1, 2, 8, 10–14]. Such materials are excellent candidates for electroactive applications and offer a wide opportunity for the development of novel nano-scale actuators, sensors, transducers, memory storage and other shape memory devices [1, 2, 6, 10–12, 15, 16].

Of all the single phase ME materials studied so far, bismuth ferrite ($BiFeO_3$) is the only material that exhibits ferroelectricity and anti-ferromagnetism at room temperature, which makes it suitable for room temperature magneto-electric applications [1, 5, 17]. However, the bulk form of synthesized $BiFeO_3$ has weak magnetization and inhomogeneity, giving rise to leakage current, so that it is difficult to observe the ferroelectric loops [15–18]. The low saturation magnetization of bulk $BiFeO_3$ is attributed to the residual moment arising from a canted spin structure [16, 19]. To address this issue,

[5] Author to whom any correspondence should be addressed.

most studies have concentrated on fabricating nanostructured $BiFeO_3$ [6, 12, 15, 20]. Nano-sized $BiFeO_3$ particles display strong size-dependent magnetic properties [5, 18]. Moreover, when the $BiFeO_3$ particle size is reduced to below that of the periodicity of helical ordering, the modulated spin structure is suppressed and the magnetization in nano-particles is improved [5, 18].

In this study, we concentrate on fabricating nanostructured $BiFeO_3$ in the form of fibers using a sol–gel method in combination with the electrospinning technique. The preparation of the inorganic $BiFeO_3$ fibers involves the following steps: (a) prepare precursor $BiFeO_3$ sol solution and electrospinning solution with an appropriate polymer concentration, (b) add the sol precursor solution to the electrospinning solution and electrospin to obtain the inorganic/organic composite fibers, and then (c) thermally anneal the spun fibers to yield phase pure $BiFeO_3$ fibers. The obtained structures consist of fine particles of $BiFeO_3$ that are self-assembled and self-organized as fibrous structures. Hence, we demonstrate that electrospinning is a useful means to fabricate one-dimensional multiferroic fibers of $BiFeO_3$. In fiber form, $BiFeO_3$ is suitable for many applications, such as electromagnetic devices and nanosystems, since the fibers can be arranged to form ordered macro-structural arrays, which serve as promising building blocks. Also, it is shown that the magnetic permeability of the material in fiber form can be much larger than the same volume of material in thin film form [21].

In another study, we obtained $BiFeO_3$ fibers of defined size and geometry by controlling the electrospinning parameters and investigated the fiber size effect on their ME properties. Finer fibers are composed of finer $BiFeO_3$ particles. This, in turn, affects their domain structure and enhances their ferromagnetism and ferroelectricity.

2. Experimental section

Bismuth ferrite ($BiFeO_3$) fibers were prepared using the electrospinning technique as follows. First, a sol–gel solution, referred to as solution A, was prepared by dissolving 4 g of $Bi(NO_3)_3{\cdot}5H_2O$ and 3.03 g of $Fe(NO_3)_3{\cdot}9H_2O$ in 10 ml of 2-methoxyethanol. The solution pH was adjusted to 3.0–4.0 by adding 0.05 ml ethanolamine. 5 ml of glacial acetic acid was added to control the solution viscosity [20]. The solution was then stirred for ∼2 h at room temperature. A second solution, solution B, was prepared by adding 2 g of polyvinyl pyrrolidone (PVP) with molecular weight (MW) = 360 000 to 11 g of dimethyl formamide (DMF)/ethanol (1:1 wt/wt) solvent mixture. The solution was mechanically stirred for about 1 h. Solution A was then added drop by drop to solution B under constant stirring condition to obtain homogeneous $BiFeO_3$ precursor solution for the electrospinning process.

A nanofiber electrospinning unit (NEU) purchased from Kato Tech Co., Ltd (Japan) was used to obtain $BiFeO_3$ fibers using the $BiFeO_3$ precursor solution. Electrospinning was conducted at 20 kV, ∼15 cm spacing between needle tip and collector, and a feed rate of 0.1 mm min^{-1}. The as-spun fibers obtained were dried in an oven at 100 °C for 1 h followed by thermal annealing at 600 °C in a furnace for 2 h in an air atmosphere. The resultant fibers were pure $BiFeO_3$ fibers. Additionally, the fibers were also collected onto the Pt-coated silicon substrate to facilitate subsequent AFM study.

A field emission scanning electron microscope (FESEM) was used to characterize the fiber samples and to determine the average diameter of the fibers. Both the as-spun fiber samples and the thermally annealed samples were sputter-coated with gold and examined at an accelerating voltage of 3–5 kV. The samples were also studied using transmission electron microscopy (TEM) with a Philips CM120 Biofilter TEM at an accelerating voltage of 120 kV. The crystal structures of the $BiFeO_3$ fibers were determined from the x-ray diffraction (XRD) patterns of the samples recorded using a Siemens D6000 x-ray diffractometer with Cu Kα radiation (λ = 1.54 Å). Tests were conducted in reflection mode at ambient temperature with 2θ varying between 10° and 80°. The scanning speed was 1° min^{-1} and the step size was 0.02°.

Measurements of the field-dependent magnetization for the $BiFeO_3$ fibers were characterized using a commercial Quantum Design magnetic property measurement system (MPMS) and physical property measurement system (PPMS). The magnetic field was ramped at ambient temperature (300 K) from 10 000 Gauss to −10 000 Gauss and back to 10 000 Gauss.

The surface topography and local ferroelectric properties of the $BiFeO_3$ fibers were studied with piezoresponse force microscopy (PFM) based on an atomic force microscope system (Cypher, Asylum Research). To apply the voltage to the sample, a conductive commercial tip cantilever system (Multi 75E-G, Budget Sensors) with a 3 N m^{-1} force constant and 75 kHz resonant frequency was used. The contact force set point was ∼50 nN and the driving frequencies were chosen near the contact resonance to boost the piezoresponse signals by using a dual-frequency resonance-tracking technique [22].

3. Results and discussion

The surface morphology of the as-spun fibers and $BiFeO_3$ fibers is evaluated using scanning electron microscopy (SEM). Figures 1(a) and (b) show the SEM images of as-spun fibers and thermally annealed $BiFeO_3$ fibers, respectively. It is evident from figure 1 that both the as-spun and annealed $BiFeO_3$ fibers are found to have a continuous surface microstructure. The SEM image of the $BiFeO_3$ fibers (figure 1(b)) displays continuous fine grained structures and elucidates the grain growth phenomenon. These grains are closely packed, dense, self-assembled and self-organized to yield the fiber morphology. Also, the SEM micrographs of the samples reveal that the $BiFeO_3$ fibers have much smaller diameters compared to the as-spun fibers. The average diameter of the as-spun fibers is 550 ± 200 nm whereas that of the annealed $BiFeO_3$ fibers is 180 ± 75 nm. The reduction in diameter can be attributed to the thermal treatment, which has pyrolyzed the polymer at 600 °C. The narrow distribution of fiber size also indicates that the $BiFeO_3$ fibers are composed of relatively uniform-sized grains. Transmission

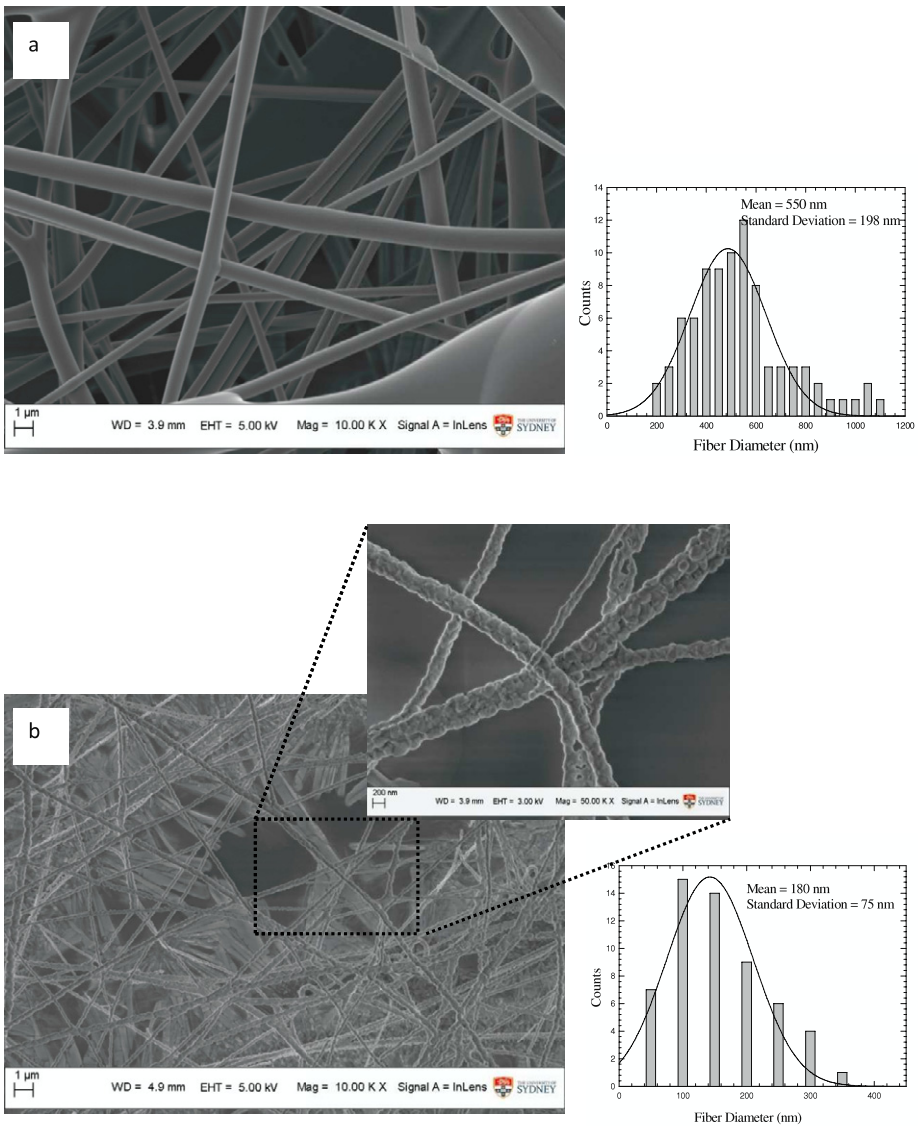

Figure 1. SEM micrographs of (a) as-spun fibers and (b) thermally annealed $BiFeO_3$ fibers. An average fiber diameter for both samples is determined using these SEM micrographs. The thermally annealed $BiFeO_3$ fibers have smaller diameters compared to the as-spun fibers. (This figure is in colour only in the electronic version)

electron microscopy (TEM) is used to further examine the microstructure and determine the grain size of the $BiFeO_3$ fibers. Figure 2(a) shows the TEM images of the $BiFeO_3$ fibers, and their grain size is revealed to be ∼30 nm. Thus, it is evident from the SEM and TEM micrographs (figures 1(b) and 2(a)) that the grains in the $BiFeO_3$ fibers self-assemble to give a linearly aligned array of particles. The high magnification TEM image (figure 2(b)) shows the crystalline lattice of $BiFeO_3$. The lattice spacing is measured to be 0.395 nm along the (012) plane. This may indicate the polycrystalline nature of the fabricated $BiFeO_3$ fibers.

The crystalline nature of the fibers is also identified and confirmed using XRD. Figure 3 shows the XRD patterns of the as-spun fibers and thermally annealed $BiFeO_3$ fibers. The former fibers do not show any peak that corresponds to any phase of $BiFeO_3$, indicating their amorphous nature. On the contrary, the XRD pattern of the $BiFeO_3$ fibers clearly shows intense peaks. This confirms that the annealed $BiFeO_3$ fibers obtained are polycrystalline. The XRD patterns of the $BiFeO_3$ fibers indicate that the development of the crystalline nature and grain growth are evolved after the annealing process. The XRD peaks of these fibers match the reported rhombohedral distorted perovskite structure of bismuth ferrite (JCPDS 86-1518). Thus, this shows that electrospinning combined with the sol–gel technique can be used to obtain $BiFeO_3$ fibers successfully. Along with the expected peaks assigned to the $BiFeO_3$ phase, we also observe a few minor peaks that are assigned to impurity phases such as $Bi_{36}Fe_2O_{57}$ and $Bi_2Fe_4O_9$. This, we believe, is a consequence of stoichiometry fluctuation in the fibers annealed at 600 °C, which can be diminished by annealing the sample at 600 °C in an argon atmosphere instead of air atmosphere.

In the next step, we investigate the magnetic properties of the obtained $BiFeO_3$ fibers. Figure 4 shows the magnetic hysteresis loops of the $BiFeO_3$ fibers measured at room temperature (300 K). The inset in the figure shows an

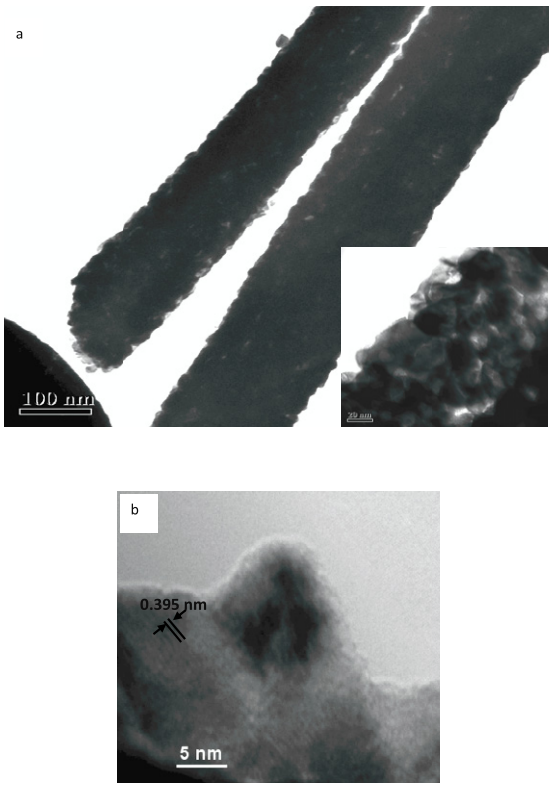

Figure 2. (a) TEM micrograph of $BiFeO_3$ fibers. The inset shows a magnified TEM image of the fibers. It is evident from the figure that the grains of $BiFeO_3$ are self-assembled and organized to yield fibrous structures. (b) High magnification TEM image of the fibers showing crystalline lattice structures.

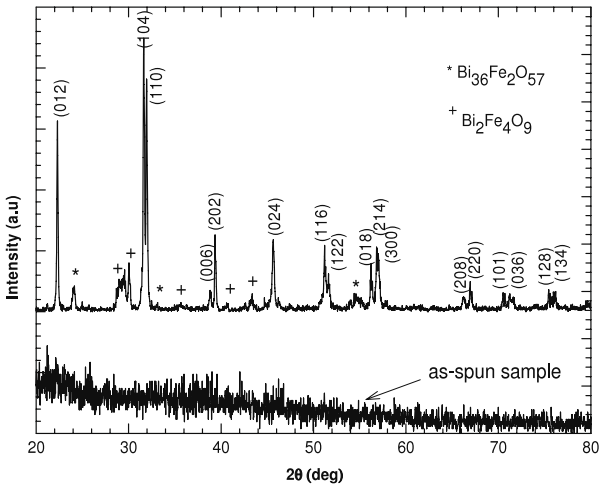

Figure 3. XRD patterns of as-spun fibers and $BiFeO_3$ fibers. The XRD patterns reveal that the as-spun fibers were amorphous in nature and crystallinity in the fibers developed due to heat treatment. The XRD peaks of the $BiFeO_3$ fibers match those of the rhombohedral distorted perovskite structure, indicating the polycrystalline nature of the $BiFeO_3$ fibers.

expanded view of the curve to highlight the opening-up of the hysteresis loop. It is evident that the sample displays sizable hysteresis; that is, the sample shows ferromagnetic order at room temperature. The nonlinearity in the M versus

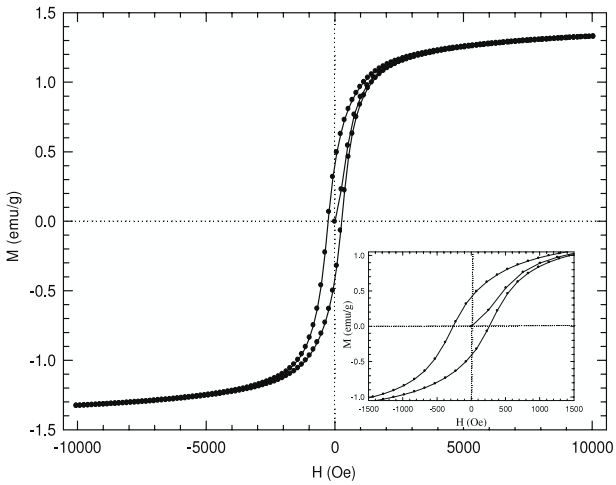

Figure 4. Magnetic hysteresis loops of $BiFeO_3$ fibers measured at 300 K, confirming the ferromagnetic behavior of the sample. The coercivity of ∼250 Oe and 1.5 emu g^{-1} saturation magnetization are determined for the sample from the hysteresis loops.

H curve (figure 4) displayed by the sample is accompanied by a coercivity of ∼250 Oe and 1.34 emu g^{-1} saturation magnetization. This is in contrast to the linear M versus H relationship commonly displayed by bulk polycrystalline $BiFeO_3$ [1, 17]. It is well known that bulk $BiFeO_3$ is associated with a disproportionate spiral spin structure, which cancels the macroscopic magnetization. Further, absence of coercivity is often noticed in bulk $BiFeO_3$ samples. Hence, the nonlinear hysteresis curve of our fibers is attributed to the nano-sized $BiFeO_3$ particles. Ferromagnetic behavior is commonly observed when the size of the particles is smaller than the size of spiral ordering [5, 12, 16], since it results in breaking of the spiral ordering, leading to ferromagnetism in the anti-ferromagnetic lattice [5, 12]. In our fibers, the $BiFeO_3$ particle size is ∼30 nm, which is much less than the size of the spiral ordering (62 nm) [5, 12, 16, 18]. Therefore, the fibers display ferromagnetic behavior.

We then use piezoresponse force microscopy (PFM) based on atomic force microscopy to investigate the ferroelectric domains and the ferroelectric behavior of the fibers at room temperature. The piezoelectric hysteresis loops are obtained by keeping the PFM tip fixed on the $BaFeO_3$ domains and applying a voltage bias across the fiber sample between a conductive AFM tip in contact with the fibers and the back electrode (Pt) of the fibers. The voltage induces local structural deformation due to a converse piezoelectric effect. The strain or piezoresponse of the sample is detected by the cantilever and acquired through a lock-in amplifier circuit. The local polarization and domain structures within the fibers are then determined from the magnitude and phase of the recorded piezoresponse. Figure 5 shows the PFM topography, near-resonance vertical PFM amplitude and phase images of a localized area on the $BiFeO_3$ fiber. The grain structure is clearly evident from the topography image (figure 5(a)), suggesting a polycrystalline structure of the $BiFeO_3$ fiber consistent with the morphology observed from TEM (figure 2) and the previous result reported by Xie *et al* [23]. Note

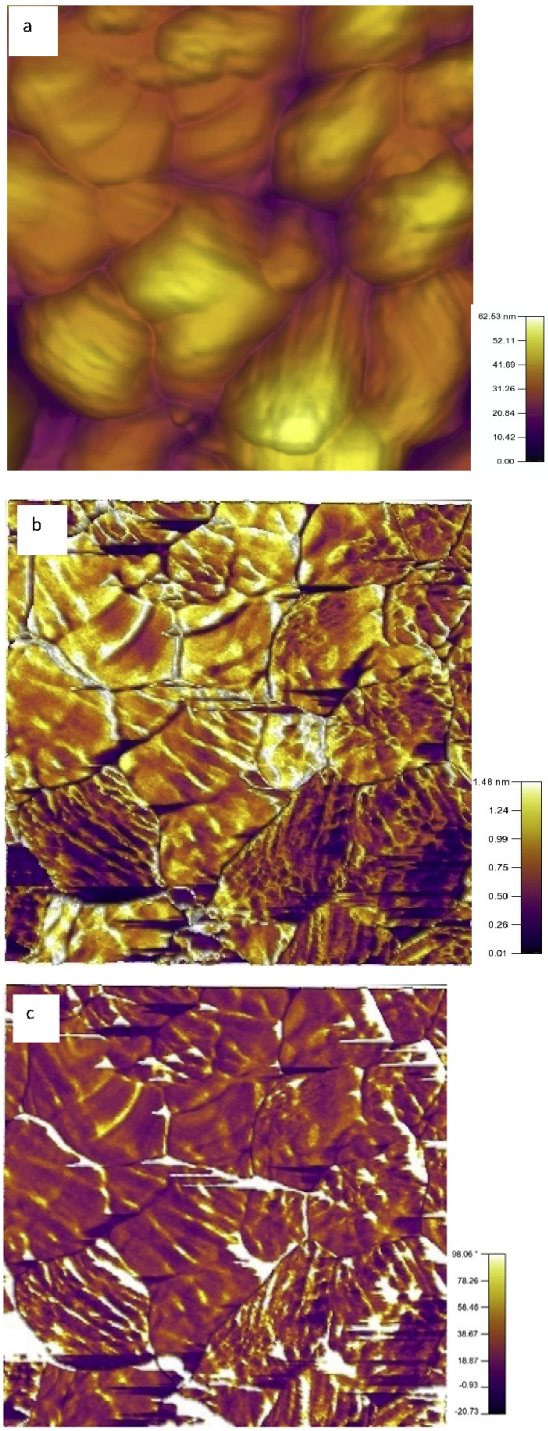

Figure 5. Piezoresponse force microscopy (PFM) of $BiFeO_3$ fibers (1 μm × 1 μm). (a) PFM topography image, (b) PFM amplitude image, and (c) PFM phase image.

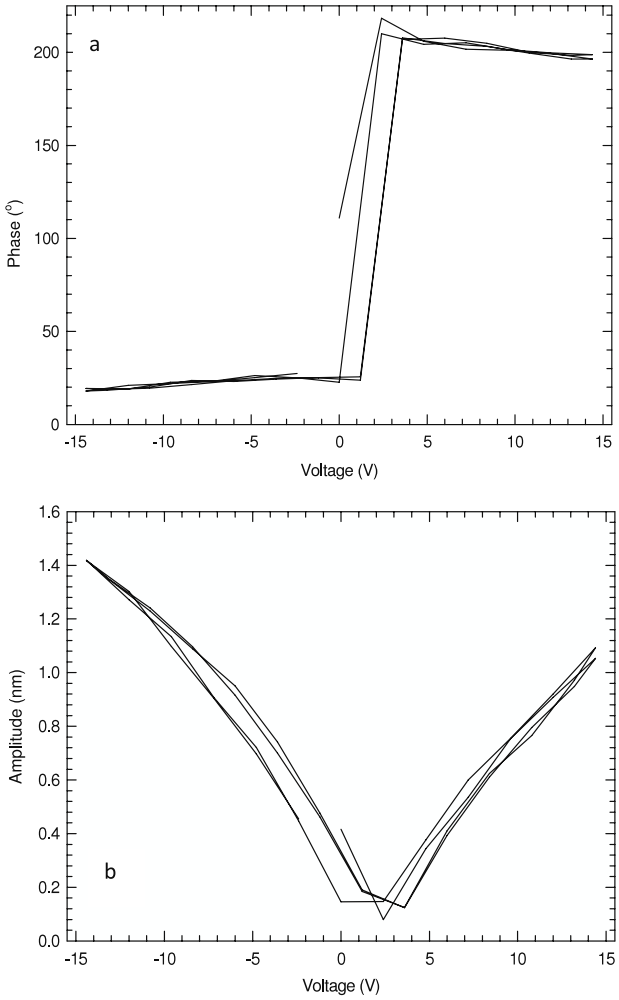

Figure 6. (a) PFM phase–voltage hysteresis loops and (b) PFM amplitude–voltage hysteresis loops.

that the fiber selected for measuring the piezoresponse has a large diameter of ∼1 μm compared to the average diameter of the fibers. This fiber was chosen as it had good contact with the Pt-coated silicon wafer, which ensured reliable PFM measurements.

The amplitude and phase images show characteristic piezoresponse of the fiber with well-defined domain structures. The amplitude image recorded (figure 5(b)) provides information on the magnitude of the piezoresponse of the domains. Figure 5(c) corresponds to the domain orientation. The contrast in these images is associated with the direction of the polarization domains. Rhombohedral $BiFeO_3$ has eight polarization vectors along ⟨111⟩ directions. Owing to the lack of crystallography orientation information about individual grains, it is difficult to assign the domain types in detail. We infer that stripe-like domain contrast is derived from the non-180° domain walls, which is also manifested in the corrugated morphology, and all the domains have a significant vertical component. It should be emphasized that the domains observed here are confined within the grain boundaries. A number of domains are involved in each grain and the size of the domains is hence less than the grain size. This is quite different from the result of Xie *et al* [23], where they claimed that the single domain can cross over the grain boundaries and the domain size is larger than the corresponding grain size. Additionally, the piezoresponse measurement is obtained by sweeping the applied DC bias whilst simultaneously measuring the response phase and amplitude signal. The response recorded for the fiber is shown in figure 6. The obtained hysteresis loops provide information about the switching behavior of the polarization

domains. Thus, figure 6(a) illustrates the polar domain switching behavior of the fibers. The phase signal shows a 180° change under the reversal of the external electric field. The amplitude loops display a butterfly shape (figure 6(b)). These are typical characteristics of ferroelectric materials. Hence, the ferroelectric behavior of the fibers is confirmed. Another feature is that the hysteresis loops in figure 6 are shifted positively along the electric field axis, implying a strong internal field within the as-fabricated fibers. This is probably caused by the asymmetric 1D fiber configuration.

4. Conclusions

One-dimensional fibrous structures of bismuth ferrite were successfully fabricated using sol–gel based electrospinning. These fibers can be relevant for the design of future nano-scale electronic devices such as sensors and actuators. The XRD analysis showed that the bismuth ferrite fibers were polycrystalline. The fibers possessed rhombohedral distorted perovskite structure, which was obtained after thermally annealing the fibers at 600 °C for ∼1 h. The ferromagnetic property of the fibers was confirmed using a physical property measurement system (PPMS). As opposed to bulk $BiFeO_3$, which demonstrates weak magnetization, the nanostructured $BiFeO_3$ in fiber form showed room temperature ferromagnetism. The fibers showed nonlinear hysteresis with coercivity of ∼250 Oe and 1.34 emu g^{-1} saturation magnetization. Further, the ferroelectricity of the fibers was confirmed using piezoresponse force microscopy. The amplitude–voltage butterfly loops and phase–voltage loops recorded for the fibers demonstrated ferroelectric hysteresis and ferroelectric switching.

Acknowledgments

We thank the Australian Research Council for the support of this work (#DP0665856). One of us (SCW) acknowledges the financial support from the US National Science Foundation under the CAREER Award CMMI #0746703.

References

[1] Wang J *et al* 2003 *Science* **299** 1719
[2] Zheng H *et al* 2004 *Science* **303** 661
[3] Wong S C, Baji A and Leng S 2008 *Polymer* **21** 4713
[4] Arinstein A, Burman M, Gendelman O and Zussman E 2007 *Nat. Nanotechnol.* **2** 59
[5] Park T J, Papaefthymiou G C, Viescas A J, Moodenbaugh A R and Wong S S 2007 *Nano Lett.* **7** 766
[6] Naumov I I, Bellaiche L and Fu H 2004 *Nature* **432** 737
[7] Reneker D H and Chun I 1996 *Nanotechnology* **7** 216
[8] Baji A, Mai Y-W, Wong S C, Abtahi M and Chen P 2010 *Comput. Sci. Technol.* **70** 703
[9] Baji A, Mai Y-W, Wong S C, Abtahi M and Du X 2010 *Comput. Sci. Technol.* **70** 1401
[10] Graeser M, Bognitzki M, Massa W, Pietzonka C, Greiner A and Wendorff J H 2007 *Adv. Mater.* **19** 4244
[11] Eerenstein W, Mathur N D and Scott J F 2006 *Nature* **442** 759
[12] Park T J, Mai Y and Wong S S 2004 *Chem. Commun.* 2708
[13] Wang Z, Suryavanshi A P and Yu M F 2006 *Appl. Phys. Lett.* **89** 082903
[14] Wu H, Zhang R, Liu X X, Lin D D and Pan W 2007 *Chem. Mater.* **19** 3506
[15] Mazumder R, Devi P S, Bhattacharya D, Choudhury P, Sen A and Raja M 2007 *Appl. Phys. Lett.* **91** 062510
[16] Sosnowska I, Neumaier T P and Steichele E 1982 *J. Phys. C: Solid State Phys.* **15** 4835
[17] Zhang S T, Lu M H, Wu D, Chen Y F and Ming N B 2005 *Appl. Phys. Lett.* **87** 262907
[18] Jaiswal A, Das R, Vivekanand K, Abraham P M, Adyanthaya S and Poddar P 2010 *J. Phys. Chem.* C **114** 2108
[19] Popov Y F, Zvezdin A K, Vorobev G P, Kadomtseva A M, Murashev V A and Rakov D N 1993 *JETP Lett.* **57** 69
[20] Liu H, Liu Z, Liu Q and Yao K 2006 *Thin Solid Films* **500** 105
[21] Shao C L, Guan H Y and liu Y C 2004 *J. Solid State Chem.* **177** 2628
[22] Rodriguez B J, Callahan C, Kalinin S V and Proksch R 2007 *Nanotechnology* **18** 475504
[23] Xie S H, Li J Y, Proksch R, Liu Y M, Zhou Y C, Liu Y Y, Ou Y, Lan L N and Qiao Y 2008 *Appl. Phys. Lett.* **93** 222904